Scattering from compact objects: Regge poles and the Complex Angular Momentum method

Mohamed Ould El Hadj,[1,2,*] Tom Stratton,[2,†] and Sam R. Dolan[2,‡]

[1] *Equipe Physique Théorique, SPE, UMR 6134 du CNRS et de l'Université de Corse, Université de Corse, Faculté des Sciences, BP 52, F-20250 Corte, France*

[2] *Consortium for Fundamental Physics, School of Mathematics and Statistics, University of Sheffield, Hicks Building, Hounsfield Road, Sheffield S3 7RH, United Kingdom*

(Dated: December 2, 2019)

To be written

CONTENTS

* m.ouldelhadj@sheffield.ac.uk
† tstratton1@sheffield.ac.uk
‡ s.dolan@sheffield.ac.uk

I. INTRODUCTION

The time-independent scattering of planar waves in the gravitational field of a compact body has been studied in some detail since the 1960s [1–3]. A substantial literature has developed on *black hole scattering*, focussing on the canonical scenario of a planar wave of frequency ω and spin s [4] impinging upon a black hole of mass M in vacuum [1–3, 5–19]. A dimensionless parameter,

$$M\omega = \pi \frac{r_g}{\lambda}, \tag{1}$$

encapsulates the ratio of the gravitational radius $r_g = 2GM/c^2$ to the wavelength λ (henceforth we adopt geometric units such that $G = c = 1$). The long wavelength ($M\omega \ll 1$), short wavelength ($M\omega \gg 1$) and intermediate regimes have been studied with a combination of perturbative [15, 20–22], semi-classical [10, 23] and numerical methods. The $s = 0$ (scalar) [2, 7, 12, 13, 24], $s = 1/2$ (fermion) [14, 18], $s = 1$ (electromagnetic) [6, 17, 25] and $s = 2$ (gravitational) cases [8, 9, 16] have all been covered.

Time-independent scattering by a compact body of radius R with a regular centre, such as a neutron star or white dwarf, has received comparatively less attention. In such a scenario, an electromagnetic wave will not penetrate inside the compact body; but on the other hand, a gravitational wave will pass through the body without impediment from the matter distribution. Similarly, a neutron star is expected to be substantially transparent to neutrinos. Though the coupling to matter is weak, the incident wave is still strongly scattered due to the influence on the spacetime curvature. Recent work [26, 27] has explored the *rainbow scattering* phenomenon that arises at short wavelengths, due to a stationary point in the geodesic deflection function associated with a ray that passes somewhat inside the body. In principle, the rainbow angle is a diagnostic of the matter distribution

of the body, and thus its nuclear equation of state.

The tenuity (inverse compactness) .

find room for [28]

Now describe the application of CAM methods to black holes, and its successes ... The aim of this work is to extend the methods to compact bodies.

Describe QNMs - resonances in the time domain: [29–35] Review of QNMs: [36]. Now describe how these are connected to Regge poles.

Finally a paragraph on the connections to Mie scattering by a transparent sphere.

[28, 37**?** , 38].

II. WAVES ON A COMPACT-BODY SPACETIME

In this section we describe the model for the compact object (II A); we introduce the effective potentials for scalar field and axial gravitational waves (II B); and we define the physical boundary conditions and the S-matrix (II C).

A. The model

The gravitating source is assumed to be spherically-symmetric, such that in a coordinate system $\{t, r, \theta, \varphi\}$, the object is described by a diagonal metric $g_{\mu\nu}$ and the line element

$$ds^2 = g_{\mu\nu}dx^\mu dx^\nu = -f(r)dt^2 + h(r)^{-1}dr^2 + r^2 d\sigma_2^2 \quad (2)$$

where $d\sigma_2^2 = d\theta^2 + \sin^2\theta d\varphi^2$ denotes the metric on the unit 2-sphere S^2. In the vacuum exterior of the star ($r > R$), the radial functions $f(r)$ and $h(r)$ depend only on M, the total mass of body: $f(r) = h(r) = 1 - 2M/r$ by Birkhoff's theorem [39]. In the interior, $f(r)$ and $h(r)$ depend on the matter distribution and equation of state (EoS).

A widely-studied model is that of a polytropic star, with an EoS $p(\rho) = \kappa\rho^{1+1/\hat{n}}$, where $\hat{n}$ is the polytropic index (see e.g. [27]). Here we shall consider a special case: an incompressible perfect fluid ball of uniform density described by Schwarzschild's interior solution for an incompressible fluid [40], with

$$\rho = \frac{M}{\frac{4}{3}\pi R^3}, \quad (3a)$$

$$p = \rho\frac{\beta(R) - \beta(r)}{\beta(r) - 3\beta(R)}, \quad (3b)$$

$$\beta(x) = \sqrt{3 - 8\pi\rho x^2} \quad (3c)$$

and metric functions

$$f(r) = \frac{1}{4}\left(1 - \frac{2Mr^2}{R^3}\right) + \frac{9}{4}\left(1 - \frac{2M}{R}\right) - \frac{3}{2}\sqrt{\left(1 - \frac{2M}{R}\right)\left(1 - \frac{2Mr^2}{R^3}\right)}, \quad (4a)$$

$$h(r) = 1 - \frac{2Mr^2}{R^3}. \quad (4b)$$

The constant-density model can be thought of as representing the $\hat{n} \to 0$ limit of the family of polytropes. The radial function $h(r)$ is C^0 at the surface of the star $r = R$ (i.e. continuous but not differentiable), and the radial function $f(r)$ is C^1 there (i.e. once-differentiable). In the polytropic cases $n > 0$, the functions are more regular (Sam: can we make a precise statement?) at the surface, but not C^∞ (i.e. not smooth). As we shall see, the breakdown of smoothness leads to consequences for the Regge pole spectrum.

We shall consider a scalar wave $\Phi(x)$ propagating on the compact body spacetime, governed by the Klein-Gordon equation

$$\Box\Phi \equiv \frac{1}{\sqrt{-g}}\partial_\mu\left(\sqrt{-g}g^{\mu\nu}\partial_\nu\Phi\right) = 0 \quad (5)$$

where $g^{\mu\nu}$ is the inverse metric and g is the metric determinant. Performing a standard separation of variables,

$$\Phi = \frac{1}{r}\sum_{\omega\ell m}\phi_{\omega\ell}(r)Y_{lm}(\theta,\phi)e^{-i\omega t}, \quad (6)$$

leads to a radial equation of the form

$$\left[\frac{d^2}{dr_*^2} + \omega^2 - V_\ell(r)\right]\phi_{\omega\ell} = 0, \quad (7)$$

where $V_\ell(r)$ is the effective potential, and r^* denotes the *tortoise coordinate* defined by

$$\frac{dr}{dr^*} = \sqrt{f(r)h(r)}. \quad (8)$$

B. Effective potentials

The effective potential for the scalar field in Eq. (7) is $V_\ell(r) = V_\ell^{(s=0)}(r)$, where we define

$$V_\ell^{(s)}(r) \equiv f(r)\left[\frac{\ell(\ell+1)}{r^2} + \frac{\beta_s\, h(r)}{2r}\left(\frac{f'(r)}{f(r)} + \frac{h'(r)}{h(r)}\right)\right], \tag{9}$$

where $\beta_s \equiv 1 - s^2$. Remarkably, the radial equation for axial gravitational perturbations is identical to Eq. (7) but with an effective potential $V_\ell^{\rm ax}(r)$ where [41]

$$V_\ell^{\rm ax}(r) = V_\ell^{(s=2)} + 8\pi f(r)(p-\rho). \tag{10}$$

Outside the star in the vacuum region ($r > R$), the effective potentials reduce to the Regge-Wheeler potential,

$$V_\ell^{(s)}(r) = \left(1 - \frac{2M}{r}\right)\left(\frac{\ell(\ell+1)}{r^2} + \frac{2M\beta_s}{r^3}\right) \tag{11}$$

with $s = 0$ in the scalar-field case, and $s = 2$ in the axial gravitational-wave case. In the exterior, the tortoise coordinates r^* reduces to $r^* = r + 2M\ln[r/(2M) - 1] + k$, where k is a constant that is chosen such that $r_*(r = 0) = 0$ and $r_*(r)$ is a continuous function.

Effective potentials for the incompressible model are shown in Fig. 1, for two cases: (i) a neutron-star model with $R = 6M$, and (ii) a ultra-compact object (UCO [42]) with $R = 2.26M$. In both cases we observe a discontinuity in $V_\ell(r)$ across the star's surface, due to the C^0 property of $h(r)$. The jump in the potential takes opposite signs in the scalar-field and gravitational-wave cases, with

$$\Delta V_\ell^{(s=0)} = +\frac{3Mf(R)}{R^3}, \tag{12a}$$

$$\Delta V_\ell^{\rm ax} = -\frac{3Mf(R)}{R^3}, \tag{12b}$$

where

$$\Delta V_\ell \equiv \lim_{\epsilon\to 0}\left\{V_\ell(R+\epsilon) - V_\ell(R-\epsilon)\right\}. \tag{13}$$

In the UCO case ($R < 3M$), the effective potential has a maximum near the light-ring at $r = 3M$, and there is a trapping region, as shown in Fig. 1.

C. Boundary conditions and scattering

The modes $\phi_{\omega\ell}$ in Eq. (6) should have a regular behaviour at the centre of the object ($r = 0$), and inspection of the radial equation (7) shows that

$$\phi_{\omega\ell}(r) \underset{r\to 0}{\sim} r^{\ell+1}. \tag{14}$$

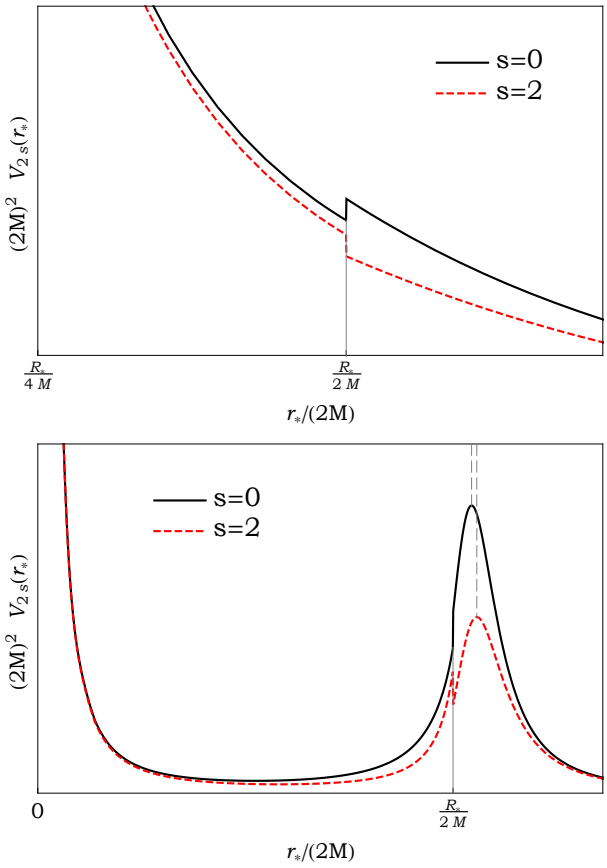

FIG. 1. The effective potential V_ℓ for a quadrupole ($\ell = 2$) perturbation of a compact body of constant density and tenuity $R/M = 6$ (upper) and $R/M = 2.26$ (lower). The scalar field potential (9) and axial gravitational-wave potential (17) are indicated as solid/black lines and dotted/red lines, respectively. The horizontal axis is the tortoise coordinate $r_*/(2M)$ defined in Eq. (8).

At the boundary of the compact object, the potential is C^0 and thus the mode is C^2. The asymptotic behaviour of the modes far from the body ($r \to +\infty$, or equivalently $r_* \to +\infty$) is

$$\phi_{\omega\ell}(r) \underset{r_*\to+\infty}{\sim} A_\ell^{(-)}(\omega)e^{-i\omega r_*} + A_\ell^{(+)}(\omega)e^{+i\omega r_*}. \tag{15}$$

With the complex coefficients $A_\ell^{(\pm)}(\omega)$ we then define the *S-matrix elements*,

$$S_\ell(\omega) = e^{i(\ell+1)\pi}\,\frac{A_\ell^{(+)}(\omega)}{A_\ell^{(-)}(\omega)}. \tag{16}$$

We now consider the poles of $S_\ell(\omega)$ in the complex plane.

III. THE REGGE POLE SPECTRUM

A. Quasinormal modes and Regge poles

Mathematically, there is a close relationship between quasinormal modes and Regge poles; they are both sets of poles of the scattering matrix. Physically, quasinormal modes are most relevant to time-dependent scattering scenarios, and Regge poles to time-independent scattering scenarios.

The *quasinormal mode spectrum* is the set of frequencies $\{\omega_{\ell n}\}$ in the complex-ω plane at which the scattering matrix $S_\ell(\omega)$ has a simple pole for a integer value of ℓ (so $\ell \in \mathbb{N}$ and $\omega_{\ell n} \in \mathbb{C}$).

The *Regge pole spectrum* is the set of angular momenta $\lambda_{\omega n} = \ell_n(\omega) + 1/2$ in the complex-λ plane at which the scattering matrix has a simple pole for a real value of ω (so $\omega \in \mathbb{R}$ and $\lambda_n(\omega) \in \mathbb{C}$). Here n is an index for enumerating the discrete spectrum of poles. In all cases considered in this work, the simple poles of $S_\ell(\omega)$ arise as simple zeros of $A_\ell^{(-)}(\omega)$.

The quasinormal mode spectrum of spherically-symmetric compact objects has been studied in some detail in Refs. [30, 32, 33, 36, 43]. Newly-formed neutron stars, the remnants of supernovae collapse, are predicted to pulsate with a large initial energy, and fluid pulsations will generate gravitational waves. In 1967, Thorne and Campolattaro [44] classified the fluid modes of a relativistic compact body by analogy with the fluid modes of a Newtonian body, with the addition of a damping time due to the emission of GWs. Two decades later, the subject was examined again [29, 30], and Kokkotas and Schutz [32] showed the existence of an additional family of modes, dubbed w-modes. These modes are characterised by a negligible excitation of fluid motion, and in the axial sector, by no fluid motion at all. They are highly damped and correspond to excitations of the dynamical perturbed space-time. For a review of (gravitational) quasinormal modes in relativistic stars and black holes see Ref. [36].

The w-modes (quasinormal modes) may be divided into three branches:

1. Curvature modes, oscillations whose damping is larger for less compact bodies. (Sam: Anything else to say on curvature modes?)

2. Interface modes ($\omega_{\rm II}$-modes [33]), characterised by very rapid damping (i.e. large negative imaginary part of $\omega_{\ell n}$). This branch of modes is most similar to the Schwarzschild black hole quasinormal modes.

3. Trapped modes [31]: These modes exist for UCOs with $R/M < 3$, because the effective radial potential has a local minimum inside the star, and local maximum near the photon sphere $r = 3M$. The number of trapped modes increases with the depth of the potential well, and the damping rate decreases.

For more details on quasinormal modes see (Sam: Appropriate reference needed.)

We now turn our attention to calculating the Regge pole spectrum for compact bodies.

B. Numerical method

In order to determine the Regge poles we adapt the method of Benhar, Berti and Ferrari (BBF), described in Sec. 4 of Ref. [45]. In turn, the BBF method is an adaptation of the *continued fraction method* developed by Leaver in the case of black hole-quasinormal mode frequencies [46]. Though BBF used the method to find axial QNM frequencies, their method is equally valid, *mutatis mutandis*, for finding the Regge poles. We have implemented numerically this method by using the Hill determinant approach of Majumdar and Panchapakesan [47], or more precisely, by modifying their method and adapting it to our problem, *i.e.*, using it for a 4-term recurrence relation. We implemented the method with *Mathematica*.

(Sam: I think we need a little bit more detail here – how does the four-term recurrence relation arise, and where can it be found specifically?)

C. Numerical results

In this section we show numerical results for the Regge pole spectrum of a compact body, in two particular cases: (i) a neutron-star-like body with tenuity $R/M = 6$, and (ii) a UCO with tenuity $R/M = 2.26$ close to the Buchdahl bound. Results for the frequencies $M\omega = 3/2$ and $M\omega = 8$ are compared, for the scalar-field ($s = 0$) and axial GW ($s = 2$) cases.

Figure 2 shows the Regge pole spectrum for a neutron-star-like body ($R/M = 6$). We see that there are two branches of Regge poles in the first quadrant, which meet

at $\mathrm{Re}(\lambda_n(\omega)) \sim \omega b_0$, where b_0 is the impact parameter for the null ray which grazes the surface of the compact body. The axial GW $s = 2$ modes (filled markers) are typically close to their scalar-field $s = 0$ counterparts (unfilled markers), as might be anticipated from the similarities in the effective potentials for the two cases (see Fig. 1).

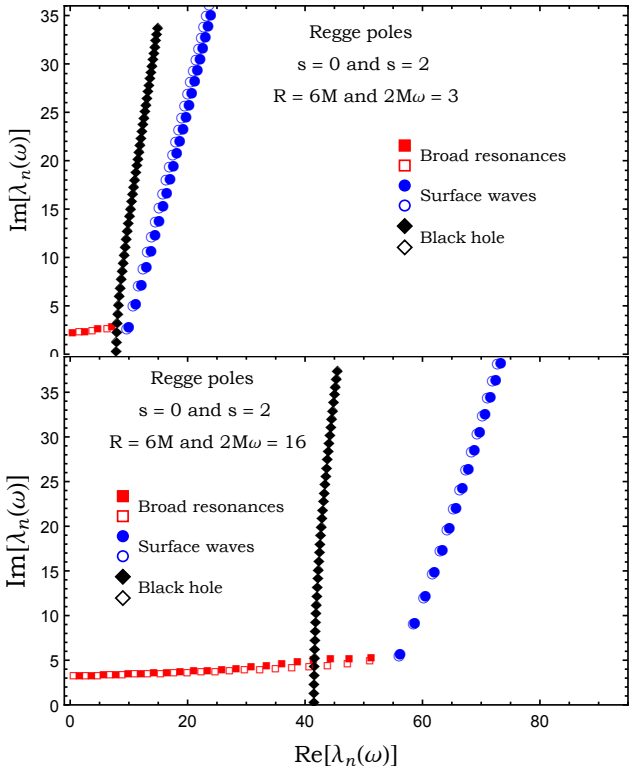

FIG. 2. The Regge poles $\lambda_n(\omega)$ for the scalar field (empty markers) and for the axial gravitational waves (filled markers).

Figure 3 shows the spectrum for a UCO with $R/M = 2.26$. These plots show evidence for an additional branch of modes that emerges from the point where the first two branches meet. The number of modes in this branch increases as the radius of the body approaches the Buchdahl limit $R \to \frac{9}{4}M$.

The Regge pole spectrum for a compact body is qualitatively similar to the Regge pole spectrum found in Mie scattering of electromagnetic waves by a transparent droplet of refractive index $\tilde{n}$. This has been studied since the 1960s; see for example Fig. 9.2 in Ref. [48]. Henceforth we shall adopt the terminology of Nussenzveig [48], in which the three branches are labelled as:

1. *Broad resonances*: approximately uniformly-spaced poles above the real axis with approximately constant imaginary part; somewhat sensitive to internal structure ($r < R$);

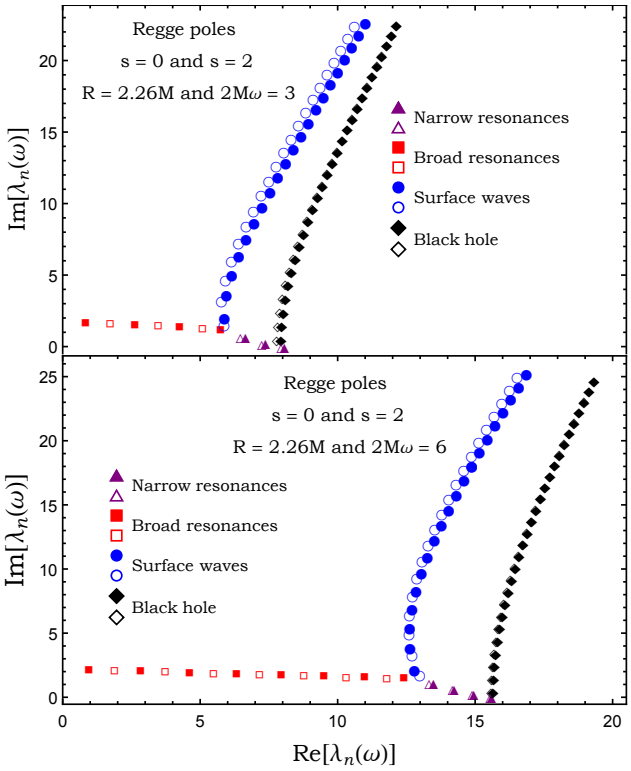

FIG. 3. The Regge poles $\lambda_n(\omega)$ for the scalar field (empty markers) and for the axial gravitational waves (filled markers).

2. *Surface waves*: highly-damped modes that are relatively insensitive to the internal structure and which depend chiefly on the surface geometry.

3. *Narrow resonances*: modes approaching the real axis corresponding to trapped modes which only appear in the UCO case ($R < 3M$).

In Figs. 2 and 3 the broad resonances, surface waves and narrow resonances are indicated by red squares, blue circles and purple triangles, respectively; and black diamonds indicate the black hole RPs. Whereas there exists an infinite number of poles of the surface-wave branch, in principle, there are no narrow-resonance poles at all in the $R/M = 6$ case, and just ≤ 4 narrow-resonance poles in the $R/M = 2.26$ case. The narrow-resonance branch is observed to end close to the start of the black-hole branch.

Data for Regge poles $\lambda_n(\omega)$ is listed in Table I (scalar field, $R/M = 6$), Table II (scalar field, $R/M = 2.26$), Table V (axial $s = 2$, $R/M = 6$) and Table IV (axial $s = 2$, $R/M = 2.26$). The values are labelled by branch (broad; surface; narrow). For the scalar field, the associated residues (see Sec.) are also presented in Tables I and Table II.

TABLE I. The lowest Regge poles $\lambda_n(\omega)$ for the scalar field and the associated residues $r_n(\omega)$. The radius of the compact bodies is $R = 6M$ and we set $2M = 1$.

n	$2M\omega$	$\lambda_n^{(\text{S-W})}{}^1(\omega)$	$\lambda_n^{(\text{B-R})}{}^2(\omega)$	$r_n^{(\text{S-W})}(\omega)$	$r_n^{(\text{B-R})}(\omega)$
1	3	$9.64850 + 2.76784i$	$1.56219 + 2.33072i$	$-12.41483 - 0.10424i$	$-0.184457 + 0.480330i$
	16	$56.00945 + 5.71038i$	$0.62529 + 3.27098i$	$-447.5395 + 25.2912i$	$-0.322061 - 0.088002i$
2	3	$10.71986 + 5.16209i$	$3.81484 + 2.48159i$	$13.8486 + 24.3824i$	$0.290952 + 1.043116i$
	16	$58.442656 + 9.18793i$	$2.64868 + 3.31439i$	$5188.750 - 859.909i$	$-0.381581 - 0.077583i$
3	3	$11.62296 + 7.17454i$	$6.35675 + 2.64104i$	$39.4189 - 12.3554i$	$2.83038 - 0.28686i$
	16	$60.20374 + 12.14965i$	$4.70011 + 3.35821i$	$-29331.71 - 18578.38i$	$-0.456423 - 0.021249i$
4	3	$12.4297 + 8.9960i$	/	$13.2301 - 50.8802i$	/
	16	$61.67700 + 14.84728i$	$6.78093 + 3.40257i$	$-15868.9 + 161199.9i$	$-0.528929 + 0.106794i$
5	3	$13.1734 + 10.6929i$	/	$-33.7366 - 51.7404i$	/
	16	$62.98626 + 17.37165i$	$8.89270 + 3.44762i$	$589920.5 - 79507.8i$	$-0.550038 + 0.330275i$
6	3	$13.8709 + 12.2989i$	/	$-66.4436 - 20.7767i$	/
	16	$64.18605 + 19.76911i$	$11.03720 + 3.49356i$	$-360464. - 1.797518 \times 10^6 i$	$-0.426365 + 0.639191i$
7	3	$14.5322 + 13.8342i$	/	$-73.0825 + 21.9088i$	/
	16	$65.30640 + 22.06743i$	$13.21653 + 3.54058i$	$-4.880638 \times 10^6 + 646112.i$	$-0.038292 + 0.926498i$
8	3	$15.1640 + 15.3122i$	/	$-56.3641 + 59.6187i$	/
	16	$66.36581 + 24.28491i$	$15.43310 + 3.5889i$	$-479098. + 1.1836070 \times 10^7 i$	$0.652285 + 0.920876i$
9	3	$15.7709 + 16.7425i$	/	$-25.0183 + 83.3731i$	/
	16	$67.37659 + 26.43447i$	$17.6898 + 3.6390i$	$2.487209 \times 10^7 + 7.72797 \times 10^6 i$	$1.363464 + 0.248276i$
10	3	$16.3565 + 18.1321i$	/	$11.7631 + 90.6815i$	/
	16	$68.34738 + 28.52564i$	$19.9900 + 3.6910i$	$3.163822 \times 10^7 - 4.265475 \times 10^7 i$	$1.29469 - 1.13096i$

[1] S-W : Surface waves
[2] B-R : Broad resonances

TABLE II. The lowest Regge poles $\lambda_n(\omega)$ for the scalar field and the associated residues $r_n(\omega)$. The radius of the compact bodies is $R = 2.26M$ and we set $2M = 1$.

n	$2M\omega$	$\lambda_n^{(\text{S-W})}{}^1(\omega)$	$\lambda_n^{(\text{B-R})}{}^2(\omega)$	$\lambda_n^{(\text{N-R})}{}^3(\omega)$	$r_n^{(\text{S-W})}(\omega)$	$r_n^{(\text{B-R})}(\omega)$	$r_n^{(\text{N-R})}(\omega)$
1	3	$5.871590 + 1.553799i$	$1.73455 + 1.64951i$	$6.48474 + 0.68765i$	$-179.7945 + 131.4187i$	$-1.52081 - 2.30968i$	$-2.5672 - 15.3797i$
	6	$12.991923 + 1.754967i$	$1.89664 + 2.13696i$	$13.34118 + 1.13496i$	$4356.193 + 647.790i$	$-0.66176 - 1.31963i$	$-390.218 + 379.906i$
2	3	$5.778805 + 3.228990i$	$3.48084 + 1.45765i$	$7.25606 + 0.24457i$	$428.6893 - 235.0321i$	$16.2123 + 5.2371i$	$-0.272250 - 1.150335i$
	6	$12.705495 + 3.383881i$	$3.74238 + 2.01309i$	$14.18757 + 0.68182i$	$-35075.99 - 9772.94i$	$-2.93679 + 4.83548i$	$-11.3519 + 34.5571i$
3	3	$5.924546 + 4.705899i$	$5.10229 + 1.29099i$	$7.95763 + 0.01764i$	$-404.6185 - 390.8531i$	$70.4849 + 54.1888i$	$-0.0370202 - 0.0048174i$
	6	$12.596259 + 4.982661i$	$5.49829 + 1.89576i$	$14.9017 + 0.2912i$	$82360.19 + 81990.53i$	$6.7872 - 16.9564i$	$0.27028 + 2.27905i$
4	3	$6.144986 + 6.043188i$	/	/	$-471.5443 + 314.3116i$	/	/
	6	$12.614598 + 6.503749i$	$7.17509 + 1.78279i$	$15.5621 + 0.0422i$	$39281.5 - 229393.2i$	$39.6176 + 33.5152i$	$0.1011154 + 0.0020569i$
5	3	$6.398427 + 7.281723i$	/	/	$37.8777 + 546.8945i$	/	/
	6	$12.71646 + 7.95208i$	$8.78112 + 1.67243i$	/	$-356055.5 + 34945.9i$	$2.1175 + 134.5962i$	/
6	3	$6.666837 + 8.447532i$	/	/	$418.7890 + 315.4209i$	/	/
	6	$12.87420 + 9.33552i$	$10.32300 + 1.56317i$	/	$45934.6 + 468157.5i$	$66.944 + 324.598i$	/
7	3	$6.941642 + 9.557619i$	/	/	$499.2703 - 37.6476i$	/	/
	6	$13.06993 + 10.66226i$	$11.80630 + 1.45720i$	/	$558619.4 + 61956.5i$	$833.855 + 78.332i$	/
8	3	$7.218463 + 10.623548i$	/	/	$367.2578 - 307.7533i$	/	/
	6	$13.29184 + 11.93979i$	/	/	$293571.8 - 559756.8i$	/	/
9	3	$7.494953 + 11.653498i$	/	/	$147.3038 - 435.8160i$	/	/
	6	$13.53197 + 13.17461i$	/	/	$-376511.5 - 570254.0i$	/	/
10	3	$7.76982 + 12.65345i$	/	/	$-71.8294 - 437.3469i$	/	/
	6	$13.78485 + 14.37216i$	/	/	$-719306.1 - 20011.7i$	/	/

[1] S-W : Surface waves
[2] B-R : Broad resonances
[3] N-R : Narrow resonances

TABLE III. The lowest Regge poles $\lambda_n(\omega)$ for the axial gravitational waves. The radius of the compact bodies is $R = 6M$ and we set $2M = 1$.

n	$2M\omega$	$\lambda_n^{(\text{S-W})^1}(\omega)$	$\lambda_n^{(\text{B-R})^2}(\omega)$
1	3	$10.004639 + 2.935907i$	$0.461101 + 2.2269826i$
	16	$56.179459 + 5.874240i$	$1.624880 + 3.2909174i$
2	3	$11.205047 + 5.343083i$	$2.551455 + 2.401243i$
	16	$58.717121 + 9.365689i$	$3.659398 + 3.336427i$
3	3	$12.166772 + 7.344219i$	$4.790413 + 2.635624i$
	16	$60.528800 + 12.332399i$	$5.722341 + 3.384112i$
4	3	$13.009174 + 9.155489i$	$7.164229 + 2.930135i$
	16	$62.040466 + 15.032415i$	$7.815081 + 3.434319i$
5	3	$13.777754 + 10.843971i$	/
	16	$63.379530 + 17.557778i$	$9.939189 + 3.487474i$
6	3	$14.494020 + 12.442853i$	/
	16	$64.603684 + 19.955393i$	$12.096463 + 3.544109i$
7	3	$15.170211 + 13.972029i$	/
	16	$65.744593 + 22.253317i$	$14.288975 + 3.604892i$
8	3	$15.814162 + 15.444717i$	/
	16	$66.821746 + 24.470040i$	$16.519109 + 3.670678i$
9	3	$16.431296 + 16.870298i$	/
	16	$67.848089 + 26.618578i$	$18.789625 + 3.742581i$
10	3	$17.025584 + 18.255740i$	/
	16	$68.832711 + 28.708547i$	$21.103712 + 3.822080i$

[1] S-W : Surface waves
[2] B-R : Broad resonances

TABLE IV. The lowest Regge poles $\lambda_n(\omega)$ for the axial gravitational waves. The radius of the compact bodies is $R = 2.26M$ and we set $2M = 1$.

n	$2M\omega$	$\lambda_n^{(\text{S-W})^1}(\omega)$	$\lambda_n^{(\text{B-R})^2}(\omega)$	$\lambda_n^{(\text{N-R})^3}(\omega)$
1	3	$5.884755 + 2.047850i$	$0.840822 + 1.728755i$	$8.0740924 + 0.022432i$
	6	$12.796673 + 2.200987i$	$0.959779 + 2.193488i$	$14.247709 + 0.699340i$
2	3	$5.960332 + 3.632211i$	$2.633309 + 1.559084i$	$7.386249 + 0.264972i$
	6	$12.640961 + 3.871470i$	$2.842316 + 2.075844i$	$14.969378 + 0.297175i$
3	3	$6.153107 + 5.055691i$	$4.262509 + 1.419601i$	$6.662827 + 0.729518i$
	6	$12.628734 + 5.440977i$	$4.629152 + 1.973668i$	$13.496329 + 1.146922i$
4	3	$6.403231 + 6.358703i$	$5.746584 + 1.200761i$	/
	6	$12.711478 + 6.932783i$	$6.330877 + 1.883529i$	$15.612017 + 0.049364i$
5	3	$6.678538 + 7.572564i$	/	/
	6	$12.859039 + 8.354930i$	$7.954922 + 1.803188i$	/
6	3	$6.964301 + 8.719285i$	/	/
	6	$13.050962 + 9.715667i$	$9.505808 + 1.730884i$	/
7	3	$7.253473 + 9.813908i$	/	/
	6	$13.273382 + 11.022841i$	$10.985288 + 1.664216i$	/
8	3	$7.542524 + 10.866909i$	/	/
	6	$13.516855 + 12.283449i$	$12.423672 + 1.572865i$	/
9	3	$7.829631 + 11.885800i$	/	/
	6	$13.774891 + 13.503511i$	/	/
10	3	$8.113848 + 12.876130i$	/	/
	6	$14.042970 + 14.688113i$	/	/

[1] S-W : Surface waves
[2] B-R : Broad resonances
[3] N-R : Narrow resonances

D. The WKB approximation

To investigate the relationship between the qualitative features of the effective potential (Fig. 1) and the three branches of Regge poles revealed in Sec. III C, we now employ the WKB method, with a view of obtain an approximation that is valid at high frequencies ($M\omega \to \infty$).

The WKB approach developed by Zhang, Wu and Leung [49] to determine the axial w-modes of a variety of stellar models can be adapted in order to obtain analytical approximations for the "broad Regge poles" for a scalar wave on a stellar background. The radial equation for axial gravitational perturbations is identical to Eq. (7) but with the potential replaced by $V_\ell \to V_\ell^{\text{ax}}$ where [41]

$$V_\ell^{\text{ax}}(r) = f(r)\left[\frac{\ell(\ell+1)}{r^2} - \frac{3h(r)}{2r}\left(\frac{f'(r)}{f(r)} + \frac{h'(r)}{h(r)}\right) + 8\pi(p-\rho)\right] \quad (17)$$

We can expect then that Regge poles for axial gravitational perturbations are qualitatively the same as for scalar perturbations, and the methods discussed can be easily adapted to deal with either case.

Regge poles and quasinormal modes for relativistic stellar models (of which w-modes are a sub-category for gravitational perturbations) both satisfy the same wave equation and the same boundary conditions but with different interpretations for the angular momentum index and the frequency. Both types of pole satisfy the regularity condition at the origin (14) and the condition of a purely outgoing wave in the far field

$$\phi^{\text{out}}_{\omega,\lambda-1/2}(r) \underset{r_*\to+\infty}{\sim} A^{(+)}_{\lambda-1/2}(\omega)e^{+i\omega r_*}. \quad (18)$$

Thus, the Regge poles are solutions of Eq. (7) for which the Wronskian of $\phi_{\omega,\lambda-1/2}$ and $\phi^{\text{out}}_{\omega,\lambda-1/2}$ vanishes (*i.e.*, $A^{(-)}_{\lambda_n(\omega)-1/2}(\omega) = 0$)

$$W[\phi_{\omega,\lambda-1/2}, \phi^{\text{out}}_{\omega,\lambda-1/2}] = 0 \quad (19)$$

It has been shown that, the asymptotic expressions of $\phi_{\omega,\lambda-1/2}$ and $\phi^{\text{out}}_{\omega,\lambda-1/2}$ can be derived in certain regions, buy using the standard WKB approximation. In the high-frequency domain we have (see Refs ...)

$$\phi_{\omega,\lambda-1/2} \underset{\omega\to\infty}{=} \omega r_* j_{\lambda-1/2}(\omega r_*) \qquad 0 \le r_* \le R_* \quad (20)$$

where $j_{\lambda-1/2}$ is the spherical Bessel function of the first kind and

$$\phi^{\rm out}_{\omega,\lambda-1/2}\underset{\omega\to\infty}{=}\begin{cases} e^{i\omega(r_*-R_*)}+\mathcal{R}e^{-i\omega(r_*-R_*)} & 1/\omega\leq r_*<R_*, \\ (1+\mathcal{R})\,e^{i\omega(r_*-R_*)} & R_*\leq r_*<\infty. \end{cases} \tag{21}$$

Here

$$R_*=\int_0^R dr\,\frac{1}{\sqrt{f(r)h(r)}} \tag{22}$$

and $\mathcal{R}$ is a reflection coefficient with the defintion given in Ref. [50]. Because the potential has a direct discontinuity at the surface of the compact body (see. Refs [49, 50] for more details), we have for our model (*i.e.*, compact body with a constant density)

$$\mathcal{R}=a\omega^{-2} \tag{23}$$

with

$$\begin{aligned} a&=-\left(\frac{i}{2}\right)^2\lim_{\epsilon\to0^+}\left[V_{\lambda-1/2}(r)\Big|_{r=R+\epsilon}-V_{\lambda-1/2}(r)\Big|_{r=R-\epsilon}\right] \\ &=\frac{3M(R-2M)}{4R^4} \end{aligned} \tag{24}$$

Now, by inserting the high frequency approximation for $j_{\lambda-1/2}(\omega r_*)$ into Eq. (20) [51],

$$\phi_{\omega,\lambda-1/2}\underset{\omega\to\infty}{\approx}-\sin\left(\frac{(\lambda-1/2)\,\pi}{2}-\omega r_*\right)\qquad 0\leq r_*\leq R_* \tag{25}$$

and Eq. (21) into the condition (19), we obtain

$$e^{i\pi(\lambda-1/2)-2i\omega R_*}=-\mathcal{R}. \tag{26}$$

We then solve Eq. (26) and we obtain

$$\lambda_n\approx\frac{2\omega R_*}{\pi}-\left(2n+\frac{1}{2}\right)+\frac{i}{\pi}\ln\left(\frac{1}{\mathcal{R}}\right) \tag{27}$$

This corresponds to the series of Regge poles with spacing $|\Delta\lambda_n|\approx2$ with the almost constant imaginary part. Of course, they lie in the first quadrant of the CAM plan with a positive real part

$$\frac{2\omega R_*}{\pi}-\left(2n+\frac{1}{2}\right)>0. \tag{28}$$

The overtones are labelled by $n=1,2,\ldots$ and n has an upper limit

$$n\leq\left\lfloor\frac{\omega R_*}{\pi}-\frac{1}{4}\right\rfloor. \tag{29}$$

In other words, there is a finite number of the "broad Regge poles".

TABLE V. The lowest Regge poles $\lambda_n(\omega)$ for the scalar field versus WKB results given by Eq. (27). The radius of the compact bodies is $R=6M$ and we assume $2M=1$.

n	ω	$\lambda_n^{\rm (B\text{-}R)}(\omega)$	$\lambda_n^{\rm (B\text{-}R,\ WKB)}(\omega)$
1	3	$1.56219+2.33072i$	$1.592793+2.189767i$
	16	$0.62529+3.27098i$	$0.661564+3.255453i$
2	3	$3.81484+2.48159i$	$3.592793+2.189767i$
	16	$2.64868+3.31439i$	$2.661564+3.255453i$
3	3	$6.35675+2.64104i$	$5.592793+2.189767i$
	16	$4.70011+3.35821i$	$4.661564+3.255453i$
4	3	/	/
	16	$6.78093+3.40257i$	$6.661564+3.255453i$
5	3	/	/
	16	$8.89270+3.44762i$	$8.661564+3.255453i$
6	3	/	/
	16	$11.03720+3.49356i$	$10.661564+3.255453i$
7	3	/	/
	16	$13.21653+3.54058i$	$12.661564+3.255453i$
8	3	/	/
	16	$15.4331+3.5889i$	$14.661564+3.255453i$
9	3	/	/
	16	$17.6898+3.6390i$	$16.661564+3.384517i$
10	3	/	/
	16	$19.9900+3.6910i$	$18.661564+3.255453i$

IV. SCATTERING AND CAM THEORY

A. The partial wave expansion

We recall that, for the scalar field, the differential scattering cross section is given by (see, e.g.,[26] and references therein)

$$\frac{d\sigma}{d\Omega}=|\hat{f}(\omega,\theta)|^2 \tag{30}$$

where

$$\hat{f}(\omega,\theta)=\frac{1}{2i\omega}\sum_{\ell=0}^{\infty}(2\ell+1)[S_\ell(\omega)-1]P_\ell(\cos\theta) \tag{31}$$

denotes the scattering amplitude. In Eq. (31), the functions $P_\ell(\cos\theta)$ are the Legendre polynomials [52]. We also recall that the S-matrix elements $S_\ell(\omega)$ appearing in Eq. (31) can be defined from the modes $\phi_{\omega\ell}$ that solve the homogenous radial equation

B. CAM representation of the scattering amplitude

To construct the CAM representation, we follow the steps in section II of the Ref [53] and recall the main results.

By using the Sommerfeld-Watson transformation [54–56] which permits us to write

$$\sum_{\ell=0}^{+\infty}(-1)^{\ell}F(\ell)=\frac{i}{2}\int_{\mathcal{C}}d\lambda\,\frac{F(\lambda-1/2)}{\cos(\pi\lambda)} \tag{32}$$

with a function F without any singularities on the real λ axis, we replace the discrete sum over the ordinary angular momentum ℓ in Eq. (31) by a contour integral in the complex λ plane (i.e., in the complex ℓ plane with $\lambda=\ell+1/2$). By noting that $P_{\ell}(\cos\theta)=(-1)^{\ell}P_{\ell}(-\cos\theta)$, we obtain

$$\hat{f}(\omega,\theta)=\frac{1}{2\omega}\int_{\mathcal{C}}d\lambda\,\frac{\lambda}{\cos(\pi\lambda)}\times\left[S_{\lambda-1/2}(\omega)-1\right]P_{\lambda-1/2}(-\cos\theta). \tag{33}$$

In Eqs. (32) and (33), the integration contour encircles counterclockwise the positive real axis of the complex λ plane, i.e., we take $\mathcal{C}=]+\infty+i\epsilon,+i\epsilon]\cup[+i\epsilon,-i\epsilon]\cup[-i\epsilon,+\infty-i\epsilon[$ with $\epsilon\to 0_{+}$ (see Fig.1 Ref [53]).

The Legendre function of the first kind $P_{\lambda-1/2}(z)$ denotes the analytic extension of the Legendre polynomials $P_{\ell}(z)$. It is defined in terms of hypergeometric functions by [52]

$$P_{\lambda-1/2}(z)=F[1/2-\lambda,1/2+\lambda;1;(1-z)/2]. \tag{34}$$

In Eq. (33), $S_{\lambda-1/2}(\omega)$ denotes "the" analytic extension of $S_{\ell}(\omega)$. It is given by [see Eq. (16)]

$$S_{\lambda-1/2}(\omega)=e^{i(\lambda+1/2)\pi}\,\frac{A^{(+)}_{\lambda-1/2}(\omega)}{A^{(-)}_{\lambda-1/2}(\omega)} \tag{35}$$

where the complex amplitudes $A^{(-)}_{\lambda-1/2}(\omega)$ and $A^{(+)}_{\lambda-1/2}(\omega)$ are defined from the analytic extension of the modes $\phi_{\omega\ell}$, i.e., from the function $\phi_{\omega,\lambda-1/2}$.

It is important to note that the poles of $S_{\lambda-1/2}(\omega)$ in the complex λ plan (i.e., the Regge poles) are defined as the zeros $\lambda_n(\omega)$ with $n=1,2,3,\ldots$ of the coefficient $A^{(-)}_{\lambda-1/2}(\omega)$ [see Eq. (35)]

$$A^{(-)}_{\lambda_n(\omega)-1/2}(\omega)=0. \tag{36}$$

The residue of the matrix $S_{\lambda-1/2}(\omega)$ at the pole $\lambda=\lambda_n(\omega)$ is defined by [see Eq. (35)]

$$r_n(\omega)=e^{i\pi[\lambda_n(\omega)+1/2]}\left[\frac{A^{(+)}_{\lambda-1/2}(\omega)}{\frac{d}{d\lambda}A^{(-)}_{\lambda-1/2}(\omega)}\right]_{\lambda=\lambda_n(\omega)}. \tag{37}$$

These residues play a central role in the complex angular momentum paradigm.

Now, we "deform" the contour $\mathcal{C}$ in Eq. (33) in order to collect, by using Cauchy's theorem, the Regge poles contributions. This is achieved by following, *mutatis mutandis*, the approach developed in Ref [53] (see more particularly Sec. IIB 3 and Fig. 1). We obtain

$$\hat{f}(\omega,\theta)=\hat{f}^{\rm B}(\omega,\theta)+\hat{f}^{\rm RP}(\omega,\theta) \tag{38}$$

where

$$\hat{f}^{\rm B}(\omega,\theta)=\hat{f}^{\rm B,Re}(\omega,\theta)+\hat{f}^{\rm B,Im}(\omega,\theta) \tag{39a}$$

is a background integral contribution with

$$\hat{f}^{\rm B,Re}(\omega,\theta)=\frac{1}{\pi\omega}\int_{\mathcal{C}_{-}}d\lambda\,\lambda S_{\lambda-1/2}(\omega)Q_{\lambda-1/2}(\cos\theta+i0) \tag{39b}$$

and

$$\hat{f}^{\rm B,Im}(\omega,\theta)=\frac{1}{2\omega}\left(\int_{+i\infty}^{0}d\lambda\,\left[S_{\lambda-1/2}(\omega)P_{\lambda_n(\omega)-1/2}(-\cos\theta)-S_{-\lambda-1/2}(\omega)e^{i\pi(\lambda+1/2)}P_{\lambda_n(\omega)-1/2}(\cos\theta)\right]\lambda\right). \tag{39c}$$

The second term in Eq. (38) ,

$$\hat{f}^{\rm RP}(\omega,\theta)=-\frac{i\pi}{\omega}\sum_{n=1}^{+\infty}\frac{\lambda_n(\omega)r_n(\omega)}{\cos[\pi\lambda_n(\omega)]}\times P_{\lambda_n(\omega)-1/2}(-\cos\theta), \tag{40}$$

is a sum over the Regge poles lying in the first quadrant of the CAM plane. Of course, Eqs. (38), (39) and (40) provide an exact representation of the scattering amplitude $\hat{f}(\omega,\theta)$ for the scalar field, equivalent to the initial partial wave expansion (31). From this CAM representation, we can extract the contribution $\hat{f}^{\rm RP}(\omega,\theta)$ given by (40) which, as a sum over Regge poles, is only an approximation of $\hat{f}(\omega,\theta)$, and which provides us with an approximation of the differential scattering cross section (30).

V. RECONSTRUCTION OF DIFFERENTIAL SCATTERING CROSS SECTIONS FROM REGGE POLE SUMS

In this section, we compare the partial wave expansions of the differential scattering cross sections with their equivalent CAM representations or, more precisely, their Regge pole approximations.

A. Computational methods

To construct the scattering amplitude (31), the back ground integrals (39b) and (39c) as well as the Regge pole contribution (40), we use, *mutatis mutandis* the computational methods that permitted one of us, in Refs [38, 53] to consider the CAM representation for scattering of the scalar, electromagnetic and gravitational waves by Schwarzschild BH (see also Ref [26]). It is important to remark that, due to the long rang nature of the field propagating on the Schwarzschild BH (outside the compact body), the scattering amplitude (31) and the background integral (39b) suffer a lack of convergence and to overcome this problem, i.e., to accelerate the convergence of this sum and integral, we have used the method described in the Appendix of Ref [53]. We have performed all the numerical calculations by using *Mathematica* [57].

B. Results

VI. DISCUSSION AND CONCLUSIONS

ACKNOWLEDGMENTS

M. O. E. H. wish to thank Antoine Folacci for various discussions concerning this work. T.S. acknowledges financial support from EPSRC. S.R.D. acknowledges financial support from the European Union's Horizon 2020 research and innovation programme under the H2020-MSCA-RISE-2017 Grant No. FunFiCO-777740, and from the Science and Technology Facilities Council (STFC) under Grant No. ST/P000800/1.

[1] W. W. Hildreth, *The Interaction of Scalar Gravitational Waves with the Schwarzschild Metric.*, Ph.D. thesis, Princeton University (1964).

[2] Richard A Matzner, "Scattering of massless scalar waves by a schwarzschild"singularity"," Journal of Mathematical Physics **9**, 163–170 (1968).

[3] CV Vishveshwara, "Scattering of gravitational radiation by a Schwarzschild black-hole." Nature **227**, 936 (1970).

[4] P. L. Chrzanowski, R. A. Matzner, V. D. Sandberg, and M. P. Ryan, "Zero Mass Plane Waves in Nonzero Gravitational Backgrounds," Phys. Rev. **D14**, 317–326 (1976).

[5] Bahram Mashhoon, "Scattering of Electromagnetic Radiation from a Black Hole," Phys. Rev. **D7**, 2807–2814 (1973).

[6] R Fabbri, "Scattering and absorption of electromagnetic waves by a schwarzschild black hole," Physical Review D **12**, 933 (1975).

[7] Norma G. Sanchez, "Elastic Scattering of Waves by a Black Hole," Phys. Rev. **D18**, 1798 (1978).

[8] Richard A. Matzner and Michael P. Jr. Ryan, "Scattering of gravitational radiation from vacuum black holes." The Astrophysical Journal Supplement Series **36**, 451–481 (1978).

[9] F. A. Handler and R. A. Matzner, "Gravitational wave scattering," Phys. Rev. **D22**, 2331–2348 (1980).

[10] Richard A. Matzner, Cécile DeWitt-Morette, Bruce Nelson, and Tian-Rong Zhang, "Glory scattering by black holes," Phys. Rev. **D31**, 1869 (1985).

[11] J. A. H. Futterman, F. A. Handler, and R. A. Matzner, *Scattering from black holes* (Cambridge University Press, 2012).

[12] N. Andersson, "Scattering of massless scalar waves by a Schwarzschild black hole: A Phase integral study," Phys. Rev. **D52**, 1808–1820 (1995).

[13] Kostas Glampedakis and Nils Andersson, "Scattering of scalar waves by rotating black holes," Class. Quant. Grav. **18**, 1939–1966 (2001), arXiv:gr-qc/0102100 [gr-qc].

[14] Sam Dolan, Chris Doran, and Anthony Lasenby, "Fermion scattering by a Schwarzschild black hole," Phys. Rev. **D74**, 064005 (2006), arXiv:gr-qc/0605031 [gr-qc].

[15] Sam R. Dolan, "Scattering of long-wavelength gravitational waves," Phys. Rev. **D77**, 044004 (2008), arXiv:0710.4252 [gr-qc].

[16] Sam R. Dolan, "Scattering and Absorption of Gravitational Plane Waves by Rotating Black Holes," Class. Quant. Grav. **25**, 235002 (2008), arXiv:0801.3805 [gr-qc].

[17] Luis C. B. Crispino, Sam R. Dolan, and Ednilton S. Oliveira, "Electromagnetic wave scattering by Schwarzschild black holes," Phys. Rev. Lett. **102**, 231103 (2009), arXiv:0905.3339 [gr-qc].

[18] Ion I. Cotaescu, Cosmin Crucean, and Ciprian A. Sporea, "Partial wave analysis of the Dirac fermions scattered from Schwarzschild black holes," Eur. Phys. J. **C76**, 102 (2016), arXiv:1409.7201 [gr-qc].

[19] Alexander Gußmann, "Scattering of massless scalar waves by magnetically charged black holes in Einstein–Yang–Mills–Higgs theory," Class. Quant. Grav. **34**, 065007 (2017), arXiv:1608.00552 [hep-th].

[20] W. K. De Logi and S. J. Kovacs, "Gravitational Scattering of Zero Rest Mass Plane Waves," Phys. Rev. **D16**, 237–244 (1977).

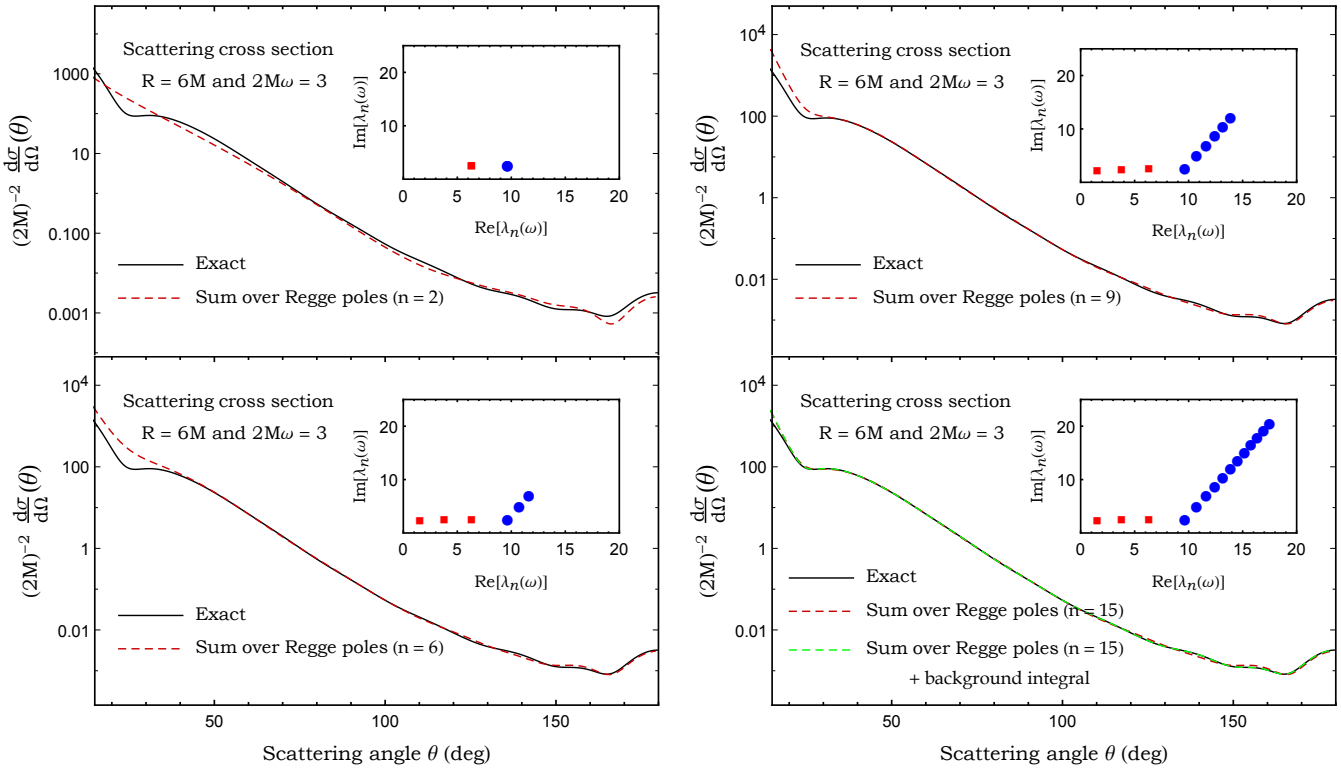

FIG. 4. The scalar cross section of a compact bodies for $2M\omega = 3$ and $R = 6M$, its Regge pole approximation and the background integral contribution.

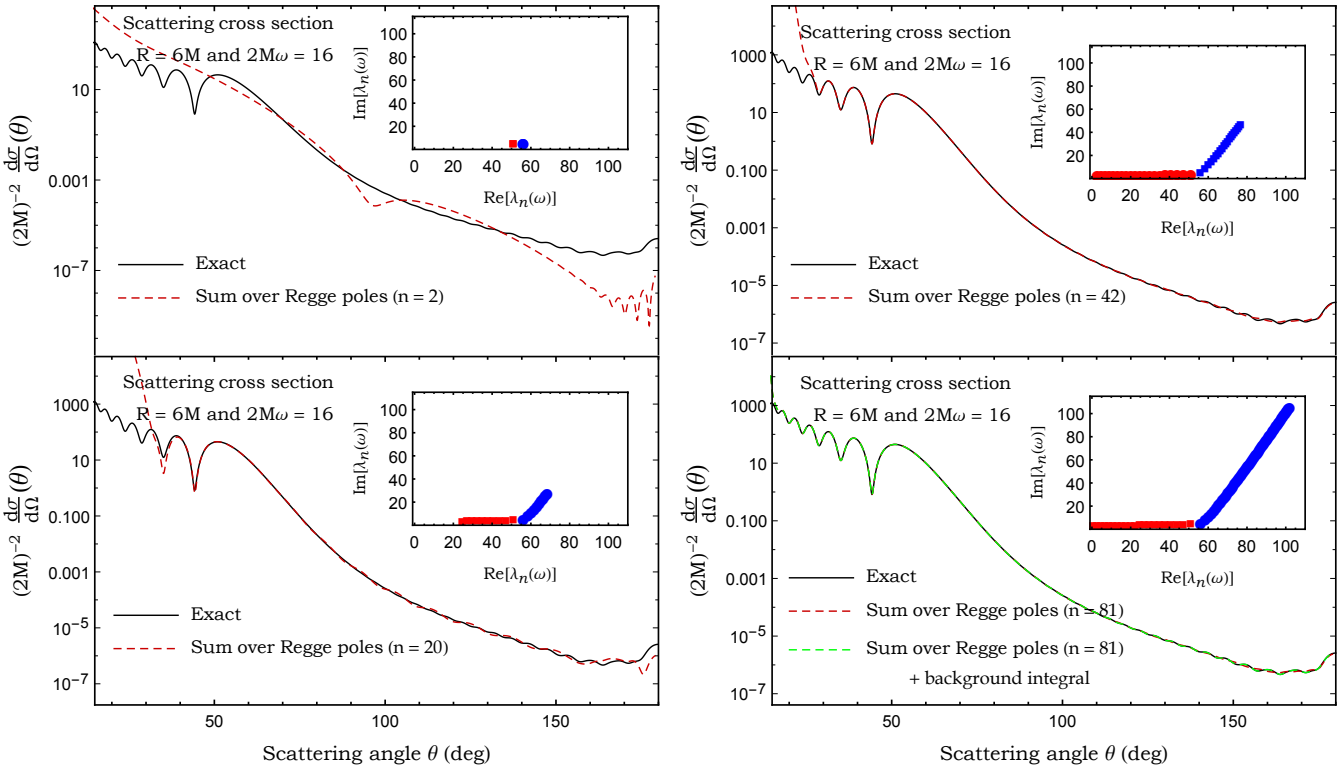

FIG. 5. The scalar cross section of a compact bodies for $2M\omega = 16$ and $R = 6M$, its Regge pole approximation and the background integral contribution.

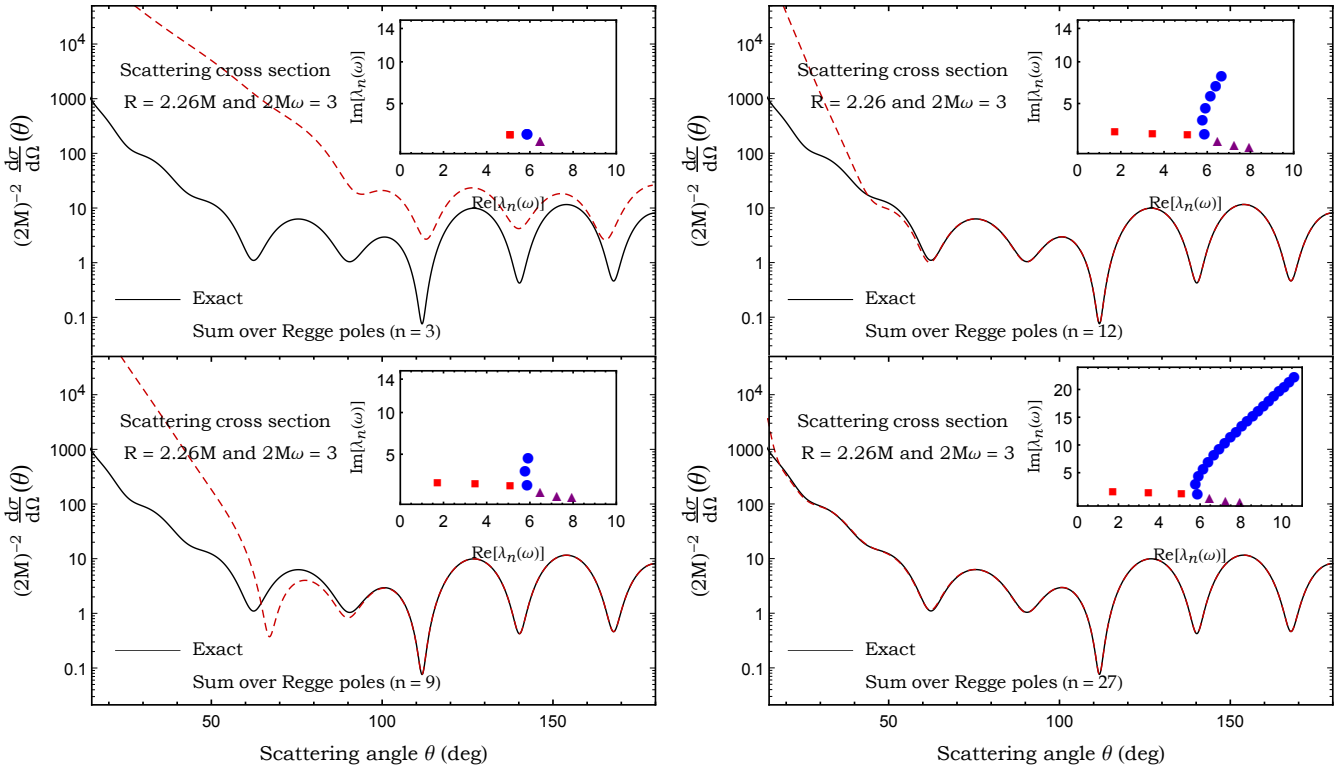

FIG. 6. The scalar cross section of a very compact bodies for $2M\omega = 3$ and $R = 2.26M$ and its Regge pole approximation.

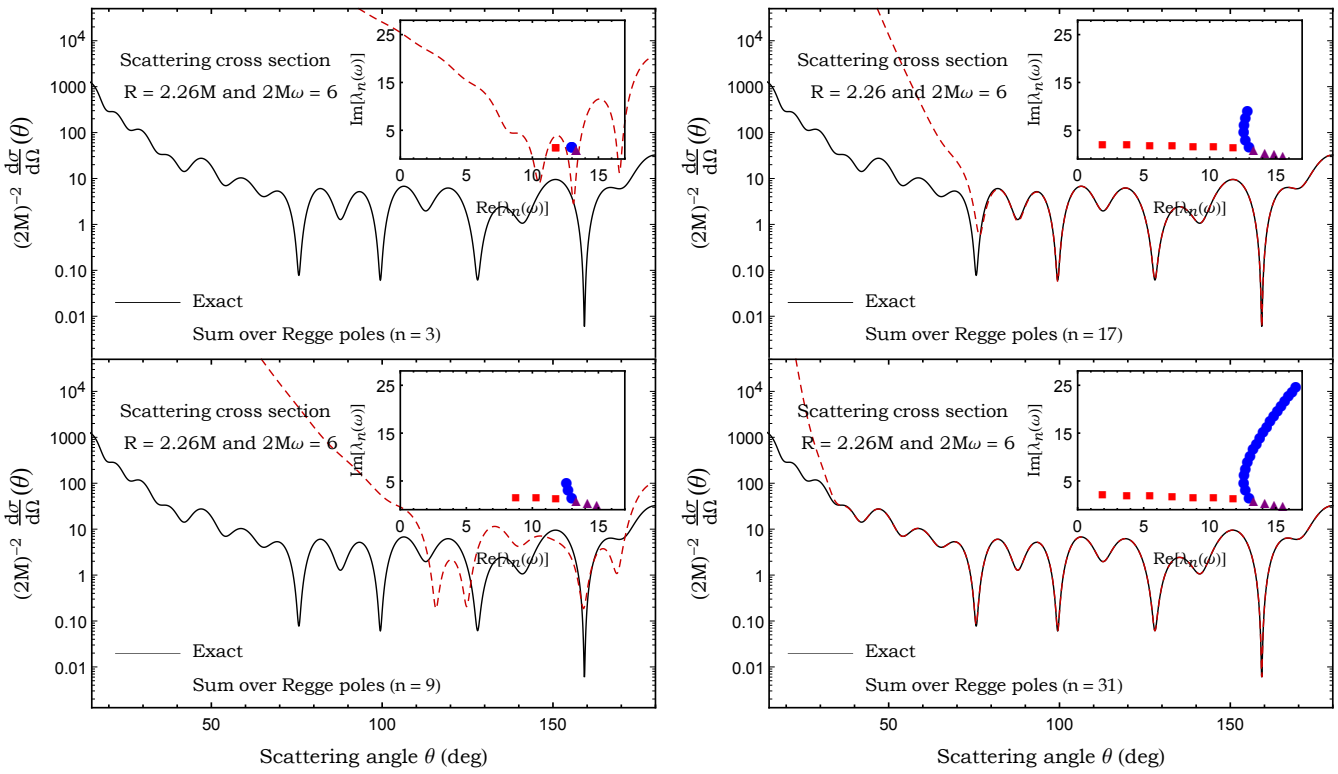

FIG. 7. The scalar cross section of a very compact bodies for $2M\omega = 6$ and $R = 2.26M$ and its Regge pole approximation.

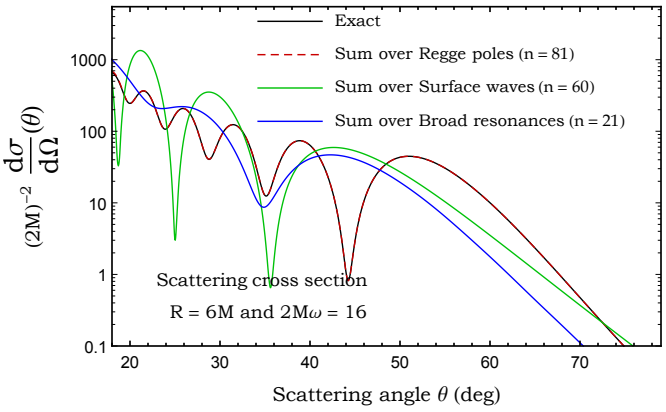

FIG. 8. Rainbow scattering for compact bodies for $2M\omega = 16$ and $R = 6M$, its Regge pole approximation and different contributions of the sum over Regge poles.

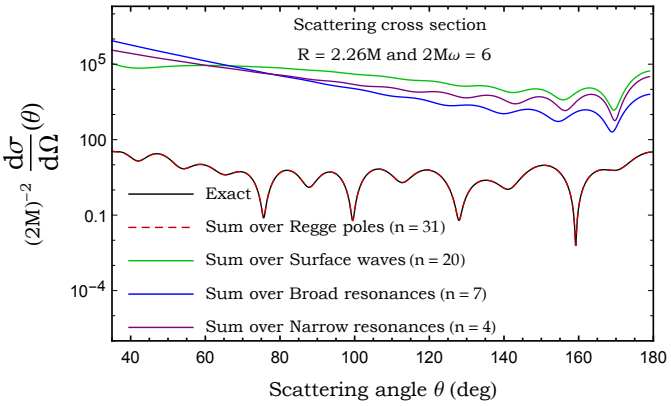

FIG. 9. Rainbow scattering for compact bodies for $2M\omega = 16$ and $R = 2.26M$, its Regge pole approximation and different contributions of the sum over Regge poles.

[21] E. Guadagnini, "Gravitons scattering from classical matter," Class. Quant. Grav. **25**, 095012 (2008), arXiv:0803.2855 [gr-qc].

[22] Francesco Sorge, "On the gravitational scattering of gravitational waves," Class. Quant. Grav. **32**, 035007 (2015).

[23] P. Anninos, C. DeWitt-Morette, R. A. Matzner, P. Yioutas, and T. R. Zhang, "Orbiting cross-sections: Application to black hole scattering," Phys. Rev. **D46**, 4477–4494 (1992).

[24] Luiz C. S. Leite, Carolina L. Benone, and Luís C. B. Crispino, "On-axis scattering of scalar fields by charged rotating black holes," Phys. Lett. **B795**, 496–501 (2019), arXiv:1907.04746 [gr-qc].

[25] Luís C. B. Crispino, Sam R. Dolan, Atsushi Higuchi, and Ednilton S. de Oliveira, "Scattering from charged black holes and supergravity," Phys. Rev. **D92**, 084056 (2015), arXiv:1507.03993 [gr-qc].

[26] Sam R. Dolan and Tom Stratton, "Rainbow scattering in the gravitational field of a compact object," Phys. Rev. **D95**, 124055 (2017), arXiv:1702.06127 [gr-qc].

[27] Tom Stratton and Sam R. Dolan, "Rainbow scattering of gravitational plane waves by a compact body," Phys. Rev. **D100**, 024007 (2019), arXiv:1903.00025 [gr-qc].

[28] Yasusada Nambu, Sousuke Noda, and Yuichiro Sakai, "Wave Optics in Spacetimes with Compact Gravitating Object," (2019), arXiv:1905.01793 [gr-qc].

[29] Steven L. Detweiler and L. Lindblom, "On the nonradial pulsations of general relativistic stellar models," Astrophys. J. **292**, 12–15 (1985).

[30] Kostas D. Kokkotas and Bernard F. Schutz, "Normal Modes of a Model Radiating System," Gen. Rel. Grav. **18**, 913 (1986).

[31] Subrahmanyan Chandrasekhar and Valeria Ferrari, "On the non-radial oscillations of a star iii. a reconsideration of the axial modes," Proceedings of the Royal Society of London A: Mathematical, Physical and Engineering Sciences **434**, 449–457 (1991), http://rspa.royalsocietypublishing.org/content/434/1891/449.full.pdf

[32] K. D. Kokkotas and Bernard F. Schutz, "W-modes: A New family of normal modes of pulsating relativistic stars," Mon. Not. Roy. Astron. Soc. **225**, 119 (1992).

[33] M. Leins, H. P. Nollert, and M. H. Soffel, "Nonradial oscillations of neutron stars: A New branch of strongly damped normal modes," Phys. Rev. **D48**, 3467–3472 (1993).

[34] Nils Andersson, Yasufumi Kojima, and Kostas D. Kokkotas, "On the oscillation spectra of ultracompact stars: An Extensive survey of gravitational wave modes," Astrophys. J. **462**, 855 (1996), arXiv:gr-qc/9512048 [gr-qc].

[35] Nils Andersson, "Two simple models for gravitational-wave modes of compact stars," General Relativity and Gravitation **28**, 1433–1445 (1996).

[36] Kostas D. Kokkotas and Bernd G. Schmidt, "Quasinormal modes of stars and black holes," Living Rev. Rel. **2**, 2 (1999), arXiv:gr-qc/9909058 [gr-qc].

[37] Luiz C. S. Leite, Sam R. Dolan, and Luís C. B. Crispino, "Absorption of electromagnetic and gravitational waves by Kerr black holes," Phys. Lett. **B774**, 130–134 (2017), arXiv:1707.01144 [gr-qc].

[38] Antoine Folacci and Mohamed Ould El Hadj, "Regge pole description of scattering of gravitational waves by a Schwarzschild black hole," Phys. Rev. **D100**, 064009 (2019), arXiv:1906.01441 [gr-qc].

[39] Nils Voje Johansen and Finn Ravndal, "On the discovery of Birkhoff's theorem," Gen. Rel. Grav. **38**, 537–540 (2006), arXiv:physics/0508163 [physics].

[40] S. L. Shapiro and S. A. Teukolsky, *Black Holes, White Dwarfs, and Neutron Stars: The Physics of Compact Objects* (Wiley, New-York, 1983).

[41] Vitor Cardoso, Luís C. B. Crispino, Caio F. B. Macedo, Hirotada Okawa, and Paolo Pani, "Light rings as observational evidence for event horizons: long-lived modes, ergoregions and nonlinear instabilities of ultracompact objects," Phys. Rev. D **D90**, 044069 (2014), arXiv:1406.5510 [gr-qc].

[42] Caio F. B. Macedo, Tom Stratton, Sam Dolan, and Luís C. B. Crispino, "Spectral lines of extreme compact objects," Phys. Rev. **D98**, 104034 (2018), arXiv:1807.04762 [gr-qc].

[43] Nils Andersson and Kostas D. Kokkotas, "Pulsation modes for increasingly relativistic polytropes," Mon. Not. Roy. Astron. Soc. **297**, 493 (1998), arXiv:gr-qc/9706010 [gr-qc].

[44] Kip S Thorne and Alfonso Campolattaro, "Non-Radial Pulsation of General-Relativistic Stellar Models. I. Analytic Analysis for L¿= 2," The Astrophysical Journal **149**, 591 (1967).

[45] Omar Benhar, Emanuele Berti, and Valeria Ferrari, "The Imprint of the equation of state on the axial w modes of oscillating neutron stars," *Gravitational waves: A challenge to theoretical astrophysics. Proceedings, Trieste, Italy, June 6-9, 2000*, Mon. Not. Roy. Astron. Soc. **310**, 797–803 (1999), [ICTP Lect. Notes Ser.3,35(2001)], arXiv:gr-qc/9901037 [gr-qc].

[46] E. W. Leaver, "An analytic representation for the quasi normal modes of Kerr black holes," Proc. Roy. Soc. Lond. A **402**, 285–298 (1985).

[47] B. Majumdar and N. Panchapakesan, "Schwarzschild black-hole normal modes using the Hill determinant," Phys. Rev. D **40**, 2568 (1989).

[48] Herch Moysés Nussenzveig, *Diffraction effects in semiclassical scattering*, Vol. 1 (Cambridge University Press, 2006).

[49] Y. J. Zhang, J. Wu, and P. T. Leung, "High-frequency behavior of w-mode pulsations of compact stars," Phys. Rev. **D83**, 064012 (2011), arXiv:1101.0319 [gr-qc].

[50] M V Berry, "Semiclassically weak reflections above analytic and non-analytic potential barriers," Journal of Physics A: Mathematical and General **15**, 3693–3704 (1982).

[51] F. W. J. Olver, D. W. Lozier, R. F. Boisvert, and C. W. Clark, *NIST Handbook of Mathematical Functions* (Cambridge University Press, 2010).

[52] M. Abramowitz and I. A. Stegun, *Handbook of Mathematical Functions* (Dover, New-York, 1965).

[53] Antoine Folacci and Mohamed Ould El Hadj, "Regge pole description of scattering of scalar and electromagnetic waves by a Schwarzschild black hole," Phys. Rev. **D99**, 104079 (2019), arXiv:1901.03965 [gr-qc].

[54] G. N. Watson, "The diffraction of electric waves by the Earth," Proc. R. Soc. London A **95**, 83 (1918).

[55] A. Sommerfeld, *Partial Differential Equations of Physics* (Academic Press, New York, 1949).

[56] R. G. Newton, *Scattering Theory of Waves and Particles*, 2nd ed. (Springer-Verlag, New York, 1982).

[57] Wolfram Research, Inc., "*Mathematica*, Version 10.0," (Wolfram Research, Inc., Champaign, IL, 2014).